1. INTRODUCTION

This paper studies the extraction of the frequency-wavenumber dispersion relations (or dispersion curves) of guided Lamb waves from a non-homogeneous medium using wave-informed decomposition techniques. Estimating dispersion curves is useful in applications that involve analysing guided wave propagation in materials to estimate properties of the material, such as temperature distribution, and astress distribution correlated to dispersion curves. Numerous methods have been proposed to estimate dispersion curves from wave propagation data. One approach is to compute two-dimensional Fourier transform of data collected from uniform, linear array. This approach has been extended to incorporate compressive sensing for a sparsely separated array of transducers across a structure. This method was further extended to two-dimensions (in space), anisotropic wave propagation, structure with surrogate, temporal undersampling and wave propagation with multi-path propagation.

However, none of these methods are easily extendable to non-homogeneous materials and irregular geometries. To tackle these issues, we estimate dispersion curves on the basis of learning the underlying wave-physics. This is achieved by wave-informed decompositions. The wave-informed decomposition is a physics-informed machine learning method that utilizes ideas from mathematical physics, matrix factorizations, mathematical optimization theory and signal processing to learn modes of wave propagation in a structure.

This work identifies signal processing as a bridge between matrix factorization, wave physics and optimization theory. Specifically, it identifies a Butterworth filter that naturally arises in solving the optimization problem – this is a unique aspect of wave-informed decomposition algorithm. The filtering aspect makes the algorithm interpretable. We utilize algorithms in optimization theory that have global guarantees making our algorithms globally optimal in some conditions. The mathematical connections this work makes helps in further extending the mathematical framework discussed in this work to other linear partial differential equations and create generalized concept of filtering on domains defined by parameters of partial differential equations.

We extract dispersion curves through wave-informed decomposition algorithm for simulated ultrasonic guided waves sensed over a non-homogeneous material. We consider simulated data for a setup shown in Fig 1.

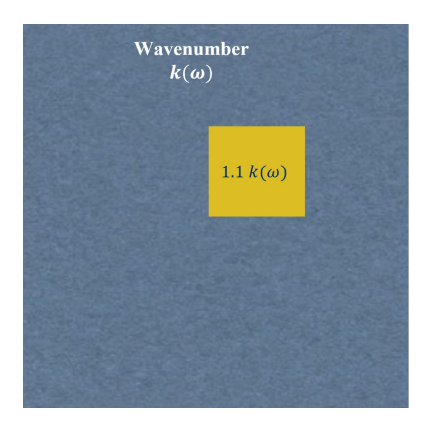


Figure 1: Non-homogeneous material setup

Our results show recovery of dispersion curves present in the data for each material in the setup. The average root mean square error (RMSE) over the four dispersion curves (two of each S0 and A0) estimated is 0.3912.

FORMULATION AND METHODOLOGY



Figure 2: Representation of 3-D Wavefield data

Consider f(x, y, t) as the sensed ultrasonic wave across a non-homogeneous material. Let its discretized version be represented by a 3-D tensor $\bar{\mathbf{X}} \in \mathbb{R}^{n_1 \times n_2 \times n_3}$ where n_1, n_2 and n_3 represent the number of points uniformly sampled in the two spatial dimensions and one time dimension respectively. To compute dispersion curves we have to first separate spatial modes for each frequency and estimate the wavenumbers corresponding to each spatial mode. To obtain wavenumbers for each frequency component, we consider the data setup where we take the Fourier transform over the time dimension of the wavefield tensor and represent it as $\hat{\mathbf{X}} \in \mathbb{R}^{n_1 \times n_2 \times n_3}$, this is represented in Fig 2. We denote $\hat{\mathbf{X}}(\omega) \in \mathbb{R}^{n_1 \times n_2}$ as the spatial variation at a fixed frequency ω . Let $\{\hat{\mathbf{D}}_i(\omega)\}_{i=1}^N$ be N spatial modes in the wavefield. We wish to approximate:

$$\hat{\mathbf{X}}(\omega) \approx \sum_{i=1}^{N} \hat{\mathbf{D}}_{i}(\omega) \tag{1}$$

Now the idea of spatial mode separation is to make sure that each $\hat{\mathbf{D}}_i(\omega)$ corresponds to a single wavenumber. For this we derive a relation from the acoustic wave equation and enforce it along with (1) to form an objective function and solve an optimization problem. In the continuous domain, the acoustic wave equation for a wave g(x, y, t) traveling at a velocity c is given by (2).

$$\nabla^2 g(x, y, t) = \frac{1}{c^2} \frac{\partial^2 g(x, y, t)}{\partial t^2}$$
 (2)

An assumption we make for our algorithm is that for each component corresponding to a velocity of propagation, the space and time are separable, i.e., for the velocity c we have, g(x,y,t)=r(x,y)h(t). After substituting the above into (2) and taking the Fourier transform in time on both sides, we get the Helmholtz equation (which is independent of time). This is defined by,

$$\nabla^2 r(x,y)h(t) = \frac{r(x,y)}{c^2} \frac{\partial^2 h(t)}{\partial t^2}$$
(3)

$$\nabla^{2} r(x,y) h(t) = \frac{r(x,y)}{c^{2}} \frac{\partial^{2} h(t)}{\partial t^{2}}$$

$$\nabla^{2} r(x,y) H(\omega) = \frac{-\omega^{2}}{c^{2}} r(x,y) H(\omega)$$
(4)

$$\nabla^2 r(x,y) = -k^2 r(x,y), \text{ when } H(\omega) \neq 0$$
 (5)

where k is the wavenumber associated with the material. We now discretize this to obtain a condition for the selection of $\hat{\mathbf{D}}_i$ in (1). For this we note from the numerical methods literature that ∇^2 in two-dimensions can be approximated with Laplacian matrices in the length and width dimensions. Now this translates in the discrete domain to:

$$\frac{1}{\Delta^2} \left(\hat{\mathbf{D}}_i(\omega) \mathbf{L}_x + \mathbf{L}_y \hat{\mathbf{D}}_i(\omega) \right) = -k^2 \hat{\mathbf{D}}_i(\omega)$$
 (6)

where Δ corresponds to the spatial resolution (sampling interval in space assuming it is the same for length and breadth dimensions) and \mathbf{L}_x and \mathbf{L}_y denote the discrete second derivative (or the discrete Laplacian) operator in length and breadth domains respectively. To simplify the math, we can assume $\Delta=1$. We can also drop the dependence on ω in notation, since we will be doing this for all frequencies and show all the calculations for one frequency. Now denote $\operatorname{vec}\left(\hat{\mathbf{D}}_i\right) \equiv \mathbf{D}_i$ and $\operatorname{vec}\left(\hat{\mathbf{X}}\right) \equiv \mathbf{X}$, the vectorized quantity such that $\mathbf{D}_i, \mathbf{X} \in \mathbb{R}^{n_1 n_2}$. Now we use vectorization properties to obtain an even compact notation for (6).

$$-k_i^2 \operatorname{vec}(\hat{\mathbf{D}}_i) = \operatorname{vec}\left(\hat{\mathbf{D}}_i \mathbf{L}_x + \mathbf{L}_y \hat{\mathbf{D}}_i\right)$$
(7)

$$-k_i^2 \mathbf{D}_i = \operatorname{vec}\left(\hat{\mathbf{D}}_i \mathbf{L}_x\right) + \operatorname{vec}\left(\mathbf{L}_y \hat{\mathbf{D}}_i\right)$$
 (8)

$$= \left[\mathbf{L}_x \otimes \mathbf{I} + \mathbf{I} \otimes \mathbf{L}_y \right] \mathbf{D}_i \tag{9}$$

$$= (\mathbf{L}_x \oplus \mathbf{L}_y)\mathbf{D}_i \tag{10}$$

where \otimes and \oplus are Kroncker product and sum defined in the usual way.¹⁴ This the compact form we need is given in (10). Now we define the optimization problem to solve for each \mathbf{D}_i and k_i .

$$\min_{\mathbf{D}, \mathbf{K}, N} \|\mathbf{X} - \mathbf{D}\mathbf{1}\|_F^2 + \lambda \left(\|\mathbf{D}\|_F^2 + \frac{1}{\gamma^2} \|\mathbf{L}\mathbf{D} + \mathbf{D}\mathbf{K}\|_F^2 \right)$$
(11)

where 1 is the column vector with all 1s that matches the size of \mathbf{D} (whose columns are \mathbf{D}_i), \mathbf{K} is a diagonal matrix that contains k_i^2 as its elements, and $\mathbf{L} = \mathbf{L}_x \oplus \mathbf{L}_y$. The first term in the optimization is to enforce (1) and the last term is the physics-informed regularizer that enforces (10). The term with a Frobenius norm on the matrix \mathbf{D} is to induce a low-rank solution. A general algorithm to solve this has been discussed in, ¹⁵ which uses theory and algorithms from ¹⁶ to solve similar non-convex problems. The algorithm in ¹⁵ solves the problem to global optimality and assumes no fixed size of \mathbf{D} to start with. We, on the other hand, use similar ideas but assume the size of \mathbf{D} is known apriori. So the algorithm is globally optimal only when the size of \mathbf{D} is known. Algorithm 1 describes the wave-informed decomposition algorithm.

3. CONNECTIONS TO FILTERING IN SIGNAL PROCESSING

In this section we show an elegant mathematical connection of the last section's algorithm to filtering theory in signal processing. Let $\mathbf{L} = \mathbf{\Gamma} \mathbf{\Lambda} \mathbf{\Gamma}^{\top}$. As a side note, using elementary properties of eigenvalues, eigenvectors and Kronecker products, we can show that:

$$\mathbf{L} = (\mathbf{\Gamma}_x \otimes \mathbf{\Gamma}_y) [\mathbf{\Lambda}_x \oplus \mathbf{\Lambda}_y] (\mathbf{\Gamma}_x \otimes \mathbf{\Gamma}_y)^{\top}$$
(12)

where $\mathbf{L}_x = \mathbf{\Gamma}_x \mathbf{\Lambda}_x \mathbf{\Gamma}_x^{\top}$ and $\mathbf{L}_y = \mathbf{\Gamma}_y \mathbf{\Lambda}_y \mathbf{\Gamma}_y^{\top}$. The objective function (13) can also be converted to the domain of spectra of \mathbf{L} , in fact, the optimization problem is solved in this domain. In the \mathbf{L} -spectral domain, the objective function can be written as:

$$\min_{\bar{\mathbf{D}}, \mathbf{K}, N} \|\widehat{\mathbf{x}} - \bar{\mathbf{D}}\mathbf{1}\|_F^2 + \lambda \left(\|\bar{\mathbf{D}}\|_F^2 + \frac{1}{\gamma^2} \|\mathbf{\Lambda}\bar{\mathbf{D}} + \bar{\mathbf{D}}\mathbf{K}\|_F^2 \right)$$
(13)

The notation in the above objective function is explained in the following text. We start the algorithm with transforming the data into the domain of eigenvectors of \mathbf{L} . Denote, $\hat{\mathbf{x}} = \mathbf{\Gamma}^{\top} \mathbf{X}$, the vector \mathbf{X} in its transform domain. Note that, the inverse transform is simply defined as $\mathbf{X} = \mathbf{\Gamma} \hat{\mathbf{x}}$. Similarly, $\bar{\mathbf{D}} = \left[\hat{\mathbf{d}}_1 \cdots \hat{\mathbf{d}}_N\right]$, where $\hat{\mathbf{d}}_i = \mathbf{\Gamma}^{\top} \mathbf{D}_i$.

Algorithm 1 Wave-informed Decomposition Algorithm

- 1: Initialization: $[n, \hat{\mathbf{e}}, \bar{\mathbf{D}}_0] = [1, \hat{\boldsymbol{x}}, 0]$
- 2: while $n \leq M$ (M is the fixed number of columns of **D** that we assume) do
- 3: **Determine Optimal** k^*

$$k_n^* = \underset{k_n}{\arg \max} \|\mathbf{F}(k_n)\widehat{\mathbf{e}}\|_2$$
, where $\mathbf{F}(k) = \left[\mathbf{I} + \gamma^{-2} \left((\mathbf{\Lambda}_x \oplus \mathbf{\Lambda}_y) + k^2 \mathbf{I} \right)^2 \right]^{-1/2}$

4. Determine D

$$\operatorname{vec}\left(\bar{\mathbf{D}}_{1:n}\right) = \left[\mathbf{1}\mathbf{1}^{\top} \otimes \mathbf{I} + \lambda \mathbf{G}(\mathbf{k})^{\top} \mathbf{G}(\mathbf{k})\right]^{-1} \operatorname{vec}\left(\hat{\mathbf{x}}\mathbf{1}^{\top}\right)$$
where,

$$\mathbf{G}(\mathbf{k}) = \begin{bmatrix} \mathbf{F}(k_1)^{-1} \cdots & \mathbf{0} \\ \vdots & \ddots & \vdots \\ \mathbf{0} & \cdots & \mathbf{F}(k_n)^{-1} \end{bmatrix}$$

5: Compute ê

$$\hat{\mathbf{e}} = \hat{\mathbf{x}} - \bar{\mathbf{D}}_{1:n} \mathbf{1}$$
$$n \leftarrow n + 1$$

6: end while

In the "determine optimal k_i " step of the algorithm, the optimal k_i^* is determined by,

$$k^* = \arg\max_{k} \left\| \left[\mathbf{I} + \frac{1}{\gamma^2} \left((\mathbf{\Lambda}_{\mathbf{x}} \oplus \mathbf{\Lambda}_{\mathbf{y}}) + k^2 \mathbf{I} \right)^2 \right]^{-\frac{1}{2}} \widehat{\mathbf{e}} \right\|_2^2.$$
 (14)

Note that, $\left[\mathbf{I} + \frac{1}{\gamma^2} \left((\mathbf{\Lambda}_{\mathbf{x}} \oplus \mathbf{\Lambda}_{\mathbf{y}}) + k_i^2 \mathbf{I} \right)^2 \right]^{-\frac{1}{2}} \in \mathbb{R}^{n_1 n_2 \times n_1 n_2}$ is a diagonal matrix. Now the (ij, ij) element of the matrix is:

$$\frac{1}{\sqrt{1 + \frac{1}{\gamma^2} \left(\lambda_{x,i} + \lambda_{y,j} + k^2\right)^2}}.$$
 (15)

Assuming Dirichlet conditions, we have closed form expressions for $\lambda_{x,i}$ and $\lambda_{y,j}$:¹⁷

$$\lambda_{x,i} = -4\sin^2\left(\frac{\pi i}{2(n_1+1)}\right) \tag{16}$$

$$\lambda_{y,j} = -4\sin^2\left(\frac{\pi j}{2(n_2 + 1)}\right) \tag{17}$$

For $i \ll n_1 + 1$ and $j \ll n_2 + 1$, we have that:

$$\lambda_{x,i} = -4\sin^2\left(\frac{\pi i}{2(n_1+1)}\right) \approx -\left(\frac{\pi i}{n_1+1}\right)^2 \tag{18}$$

$$\lambda_{y,j} = -4\sin^2\left(\frac{\pi j}{2(n_2+1)}\right) \approx -\left(\frac{\pi j}{n_2+1}\right)^2$$
 (19)

Now substituting the above, we get (ij, ij) element is approximately,

$$\frac{1}{\sqrt{1 + \frac{1}{\gamma^2} \left[\left(\frac{\pi i}{n_1 + 1} \right)^2 + \left(\frac{\pi j}{n_2 + 1} \right)^2 - k^2 \right]^2}}.$$
 (20)

This means that multiplying $\left[\mathbf{I} + \frac{1}{\gamma^2}\left((\mathbf{\Lambda_x} \oplus \mathbf{\Lambda_y}) + k_i^2\mathbf{I}\right)^2\right]^{-\frac{1}{2}}$ by vector $\hat{\mathbf{e}}$ is equivalent to filtering in the transform domain. Equation (20) shows that the filtering operation is performed by a bandpass Butterworth filter in two-dimensions. The contours of the Butterworth filter that naturally arises through this are circular for small enough wavenumbers. Mathematically, equation (20) confirms the presence of circular contours as the variable in the Butterworth filter (ω in $1/\sqrt{1+\frac{\omega^2}{\gamma^2}}$) is now replaced by $(\pi i)^2+(\pi j^2)-(n+1)^2k^2$ (in the special case of $n_1=n_2=n$) and thus will attain its maximum on the locus of the circle

$$i^2 + j^2 = \frac{(n+1)^2}{\pi^2} k^2,$$

where i and j represent horizontal and vertical wavenumbers respectively, and die down eventually according to the regularization constant γ , which can be treated as the bandwidth selected by the user. An example filter contour is shown in Fig 3. The (ij,ij) element of the matrix $\left[\mathbf{I} + \frac{1}{\gamma^2}\left((\mathbf{\Lambda_x} \oplus \mathbf{\Lambda_y}) + k_i^2\mathbf{I}\right)^2\right]^{-\frac{1}{2}}$ is placed at the (i,j)th element of a matrix, which is plotted as an image. We can also replace Γ and Λ by

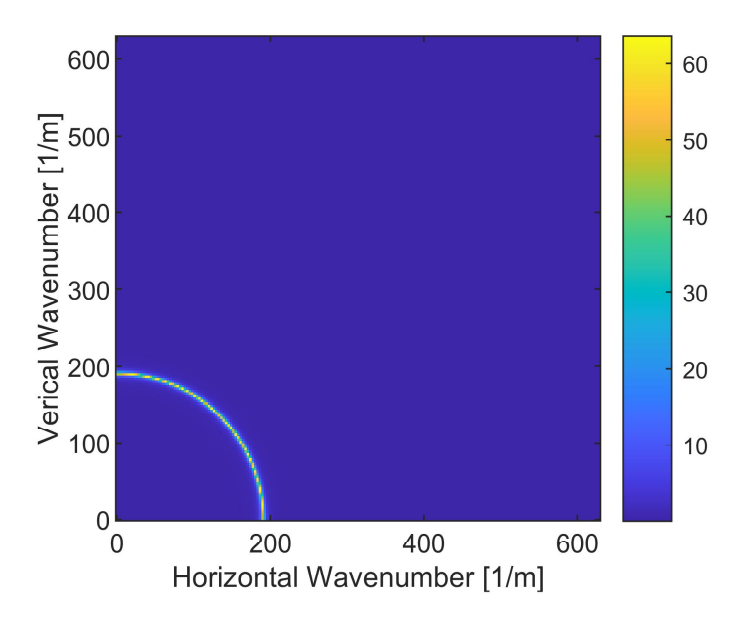


Figure 3: Representation of a bandpass Butterworth filter that naturally arises from the wave-informed decompostion algorithm

their continuous equivalents of the eigenvalues and eigenvectors of second derivatives.¹⁷ The results we show utilize eigenvalues and eigenvectors of continuous second derivative obtained from pure Neumann boundary conditions (since they impose a condition only on the derivative and do not have any condition imposed on the value of the function directly).

4. RESULTS & DISCUSSIONS

Simulated wavefield data of guided waves generated by a 50 kHz frequency pulse are measured across a 1m by 1m region of an aluminum plate with a change in wavenumber as shown in Fig 1. We show different time frames of the data in Fig 4.

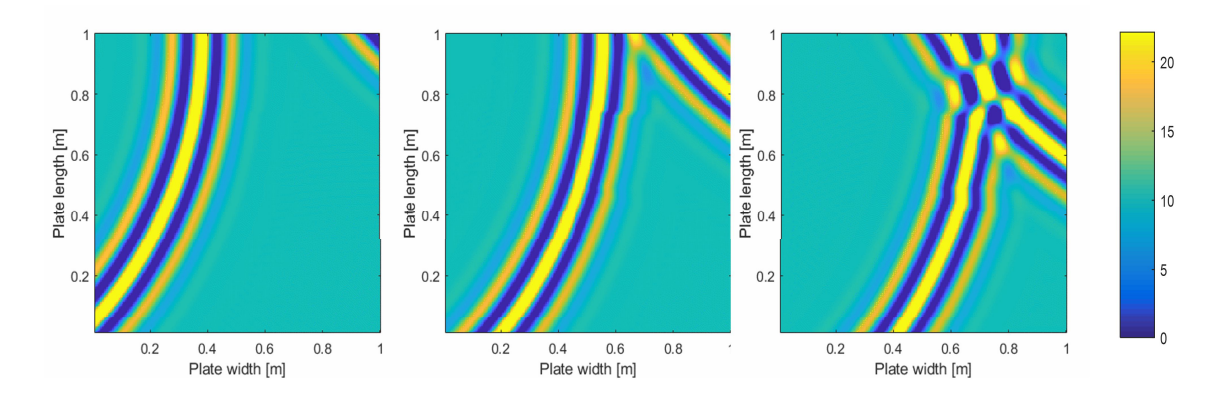


Figure 4: Wavefield at three different time shots – observe distortion at the change of material

We choose a size of 4 for the number of columns in \mathbf{D} , for sizes larger than 4, the algorithm produces dispersion curves that show dispersion at higher harmonics, we wish to illustrate our algorithm with S0 and A0 modes. We choose $\lambda=1$ to equally weigh the matrix factorization term and the regularization term, and finally we choose $\gamma=\pi^2/n^2$, where $n=n_1=n_2=200$ (which is the number of spatial points in length and breadth dimensions). The choice of the value of γ can be motivated from the Butterworth filter expression in (20). Substituting $\gamma=\pi^2/n^2$ and $n_1=n_2=n$, for large enough n where we can assume $n\approx n+1$, the bandpass Butterworth filter expression can be approximated as

$$\frac{1}{\sqrt{1+\left[i^2+j^2-\left(\frac{nk}{\pi}\right)^2\right]^2}}.$$
 (21)

Equation (21) reveals that this choice of γ ensures a -3dB cut-off wavenumber of 1m⁻¹ from the central wavenumber of the bandpass Butterworth filter.

The k_i^* obtained at each frequency is plotted against the frequency to obtain dispersion curves (see Fig. 6). In Table 1, we show RMSEs of each dispersion curve estimated for each material region. Observe that RMSE for the dispersion curves estimated for the larger region is lesser than that of the smaller region – this is due to the fact that we have more data for larger region and lesser data for the smaller region.

Dispersion Curve	RMSE $[m^{-1}]$
Large Region S0	0.1265
Small Region S0	0.5077
Large Region A0	0.1534
Small Region A0	0.7772

Table 1: Root Mean Square Errors (RMSE) between actual (S0 and A0) dispersion curves and estimated dispersion curves

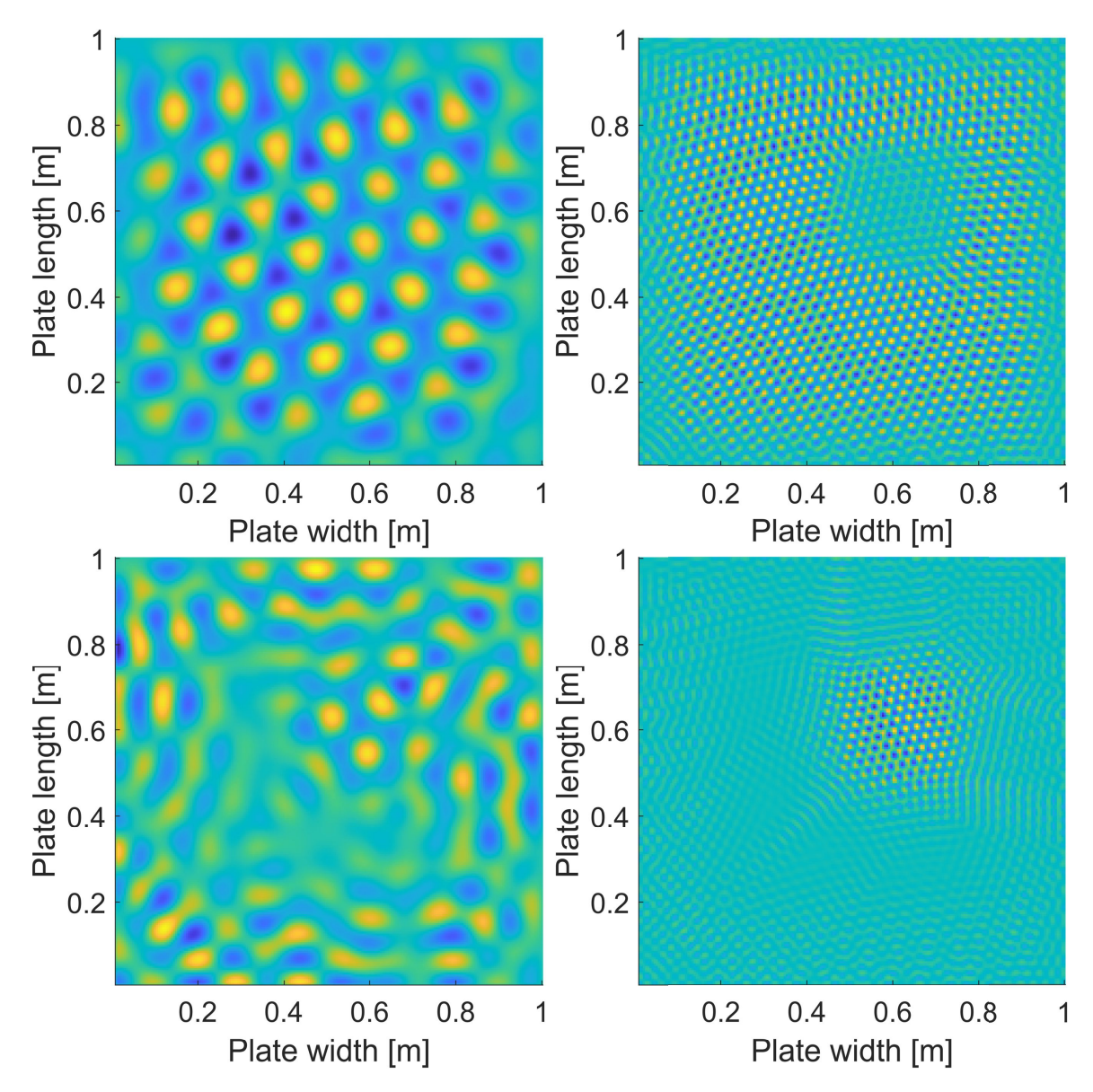


Figure 5: The four columns of D learned from the data by the wave-informed decomposition algorithm.

5. CONCLUSION

Dispersion curves were obtained as a by product of the wave-informed decomposition algorithm which was used to separate spatial modes from guided wave data in the case of wavefield measured on a non-homogeneous material. This work also can be extended to other linear partial differential equations and their corresponding spectrum and filtering operations in those domains can also be studied and utilized for various other applications that involve physical processes.

6. ACKNOWLEDGEMENTS

This material is based upon work supported by the National Science Foundation under grant no. EECS-1839704.

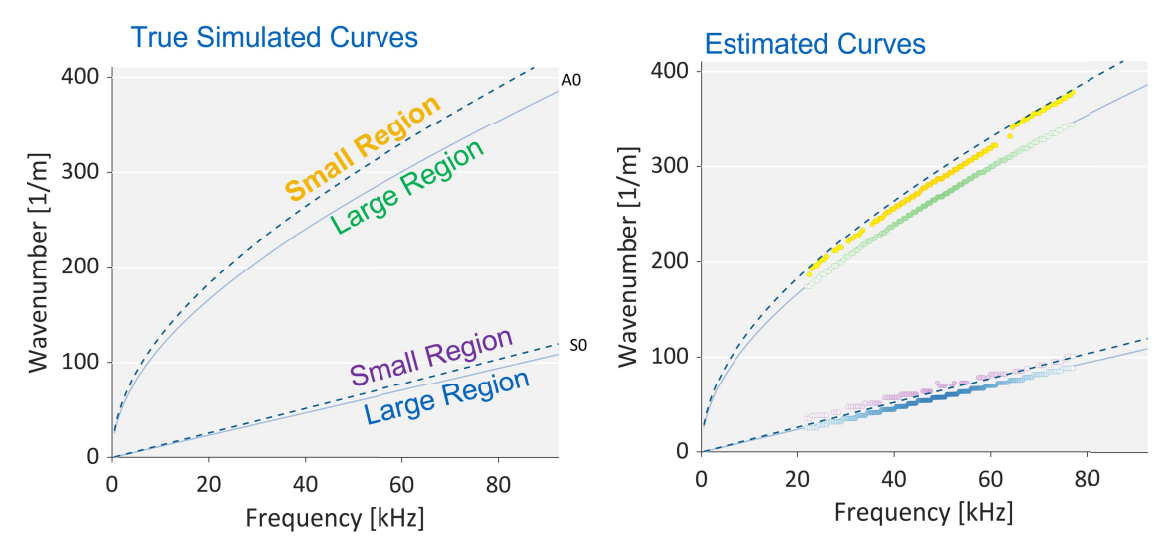


Figure 6: True dispersion curves of the simulated data (left), Estimated dispersion curves from the Wave-informed Decomposition algorithm imposed over the original dispersion curves for S0 and A0 modes(right)

REFERENCES

- ¹ H. V. Tetali, K. S. Alguri, and J. B. Harley, "Wave physics informed dictionary learning in one dimension," in *Proc. of the IEEE International Workshop on Machine Learning for Signal Processing (MLSP)*, vol. 29, 2019, pp. 1–6.
- ² A. C. S. Douglass and J. B. Harley, "Dynamic time warping temperature compensation for guided wave structural health monitoring," *IEEE Transactions on Ultrasonics, Ferroelectrics, and Frequency Control*, vol. 65, no. 5, pp. 851–861, 2018.
- ³ Y. Jia, V. Chernyshev, and M. Skliar, "Ultrasound measurements of segmental temperature distribution in solids: Method and its high-temperature validation," *Ultrasonics*, vol. 66, pp. 91–102, 2016.
- ⁴ M. Benaicha, O. Jalbaud, A. H. Alaoui, and Y. Burtschell, "Correlation between the mechanical behavior and the ultrasonic velocity of fiber-reinforced concrete," *Construction and Building Materials*, vol. 101, pp. 702–709, 2015.
- ⁵ K. Salama and C. K. Ling, "The effect of stress on the temperature dependence of ultrasonic velocity," *Journal of Applied Physics*, vol. 51, no. 3, pp. 1505–1509, 1980.
- ⁶ D. Alleyne and P. Cawley, "A two-dimensional fourier transform method for the measurement of propagating multimode signals," *The Journal of the Acoustical Society of America*, vol. 89, no. 3, pp. 1159–1168, 1991.
- ⁷ J. B. Harley and J. M. F. Moura, "Sparse recovery of the multimodal and dispersive characteristics of lamb waves," *The Journal of the Acoustical Society of America*, vol. 133, no. 5, pp. 2732–2745, 2013.
- ⁸ S. Sabeti and J. B. Harley, "Two-dimensional sparse wavenumber recovery for guided wavefields," *AIP Conference Proceedings*, vol. 1949, no. 1, p. 230003, 2018.
- ⁹ S. Sabeti, C. A. C. Leckey, L. De Marchi, and J. B. Harley, "Sparse wavenumber recovery and prediction of anisotropic guided waves in composites: A comparative study," *IEEE Transactions on Ultrasonics, Ferroelectrics, and Frequency Control*, vol. 66, no. 8, pp. 1352–1363, 2019.

- ¹⁰ J. B. Harley, "Predictive guided wave models through sparse modal representations," *Proceedings of the IEEE*, vol. 104, no. 8, pp. 1604–1619, 2016.
- ¹¹ K. S. Alguri, J. Melville, and J. B. Harley, "Baseline-free guided wave damage detection with surrogate data and dictionary learning," *The Journal of the Acoustical Society of America*, vol. 143, no. 6, pp. 3807–3818, 2018.
- ¹² S. Sabeti and J. B. Harley, "Spatio-temporal undersampling: Recovering ultrasonic guided wavefields from incomplete data with compressive sensing," *Mechanical Systems and Signal Processing*, vol. 140, p. 106694, 2020.
- ¹³ J. B. Harley, K. S. Alguri, H. V. Tetali, and S. Sabeti, "Learning guided wave dispersion curves from multi-path reflections with compressive sensing," *Structural Health Monitoring*, 2019.
- ¹⁴ A. Graham, *Kronecker products and matrix calculus with applications*. Courier Dover Publications, 2018, pp. 21–45.
- ¹⁵ H. V. Tetali, J. B. Harley, and B. D. Haeffele, "Wave-informed matrix factorization with global optimality guarantees," *arXiv preprint arXiv:2107.09144*, 2021.
- ¹⁶ B. D. Haeffele and R. Vidal, "Structured low-rank matrix factorization: Global optimality, algorithms, and applications," *IEEE Transactions on Pattern Analysis and Machine Intelligence*, vol. 42, no. 6, pp. 1468–1482, 2019.
- ¹⁷ F. Chung and S.-T. Yau, "Discrete green's functions," *Journal of Combinatorial Theory, Series A*, vol. 91, no. 1-2, pp. 191–214, 2000.